Inorg. Chem. **2009**, *48*, 574−580

Kinetics of Coloration in Photochromic Organoammonium Polyoxomolybdates

Rémi Dessapt,*,† Mathieu Collet,† Violaine Coué,† Martine Bujoli-Doeuff,† Stéphane Jobic,*,† Changhoon Lee,‡ and Myung-Hwan Whangbo*,‡

Institut des Matériaux Jean Rouxel, Université de Nantes, CNRS, 2 rue de la Houssinière, BP 32229, 44322 Nantes, France and Department of Chemistry, North Carolina State University, Raleigh, North Carolina 27695−8204, USA

Received July 24, 2008

The excellent photochromic properties of $(H_2DABCO)_2(HDMA)_{0.5}Na_{0.75}(H_3O)_{0.75}[Mo_8O_{27}]\cdot 3H_2O$ (**4**), a new member of the $(H_2DABCO)_2(A)_x[Mo_8O_{27}]\cdot nH_2O$ series, are compared with those of $(H_2DABCO)_2(NH_4)_2[Mo_8O_{27}]\cdot 4H_2O$ (**1**), $(H_2DABCO)_2(H_2pipz)[Mo_8O_{27}]$ (**2**), and $(H_2pipz)_3[Mo_8O_{27}]$ (**3**). All these powdered materials turn from white to purple under illumination at 365 nm, which is associated with photoreduction of Mo^{6+} cations into Mo^{5+} cations. We show that the rates of coloration, which increase in the order **1** < **3**, **2** < **4**, are related to the decrease in the concentration of reducible Mo^{6+} centers with irradiation time and follow a second-order reaction law because the event of light absorption at a reducible Mo^{6+} site does not necessarily coincide with that of the N^+-H bond breaking in the $N^+-H\cdots O$ hydrogen bond associated with the Mo^{6+} site. First-principles density functional electronic structure calculations were carried out to find that this trend correlates with the homolytic dissociation energies of the N^+-H bonds in the organic cations $HDMA^+$, H_2pipz^{2+}, H_2DABCO^{2+}, and NH_4^+. This observation is consistent with a photochromic mechanism based on the homolytic cleavage of N^+-H bonds rather than on the heterolytic cleavage of N^+-H bonds.

Introduction

Photochromic materials, i.e., compounds that undergo a light-induced reversible color change, have received much attention for the past three decades due to their potential industrial applications such as ophthalmic lenses, cosmetics, optical power-limiting switches, sensors, optical information storage, and smart painting. Though less extensively investigated than organic photochromes, self-assembled organic−inorganic hybrid materials based on polyoxomolybdates (POM's) and organoammonium cations[1] are considered as promising photochromic materials with a high degree of tunability in optical property as recently pointed out.[2] In general, the photogenerated colors of these compounds depend upon the chemical composition and topology of the POM's, while the coloration and fading kinetics of these compounds are related to the nature of the organoammonium cations and their $N^+-H\cdots O$ hydrogen bonds with the POM's at the organic−inorganic interface.

When irradiated at 365 nm or in daylight the colors of $(H_2DABCO)_2(NH_4)_2[Mo_8O_{27}]\cdot 4H_2O$ (**1**), $(H_2DABCO)_2(H_2pipz)[Mo_8O_{27}]$ (**2**), and $(H_2pipz)_3[Mo_8O_{27}]$ (**3**) turn progressively from yellowish-white to purple. However, the color change is much faster for **2** and **3** than for **1**.[2] In these three compounds the infinite $^1/_\infty[Mo_8O_{27}]^{6-}$ chains, made up of corner-sharing γ-$[Mo_8O_{28}]$ blocks, are well separated from each other by the cations located in two distinct lattice sites (Figure 1). For **1** and **2**, the H_2DABCO^{2+} cations occupy exclusively site 1 and the NH_4^+ or H_2pipz^{2+} cations site 2. In **3**, H_2pipz^{2+} cations are present on both sites 1 and 2. This particular site preference of the organic cations may originate from a steric reason and the ability for the organic cations with at least two N^+-H bonds per nitrogen to play the role of a pincer between successive γ-$[Mo_8O_{28}]$ subunits, hence reinforcing the stability and rigidity of $^1/_\infty[Mo_8O_{27}]^{6-}$ chain packing.[2]

It is of interest to examine the photochromism of **1**−**3** from the viewpoint of Yamase's model[1] for photochromism in

* To whom correspondence should be addressed. E-mail: remi.dessapt@cnrs-imn.fr; stephane.jobic@cnrs-imn.fr; mike_whangbo@ncsu.edu.
† Université de Nantes.
‡ North Carolina State University.

(1) Yamase, T. *Chem. Rev.* **1998**, *98*, 307–325.
(2) Coué, V.; Dessapt, R.; Bujoli-Doeuff, M.; Evain, M.; Jobic, S. *Inorg. Chem.* **2007**, *46*, 2824–2835.

10.1021/ic8013865 CCC: $40.75
Published on Web 12/19/2008

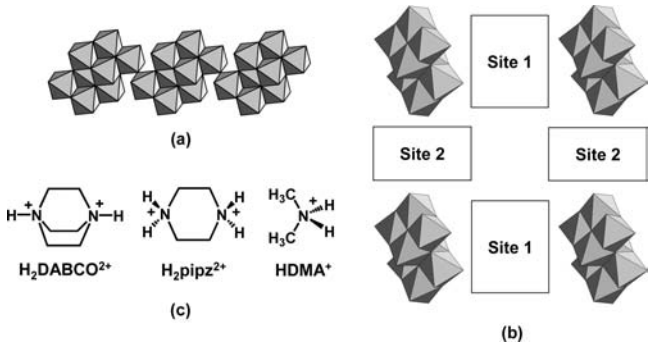

Figure 1. (a) Perspective view of $^1/_\infty[Mo_8O_{27}]^{6-}$ chains made up of discrete γ-$[Mo_8O_{28}]$ blocks connected via corner sharing. (b) Projection view of the three-dimensional crystal structure of **1**, **2**, and **3** along the $^1/_\infty[Mo_8O_{27}]^{6-}$ chains where the lattice sites 1 and 2 are occupied by countercations. (c) Representations of the H_2DABCO^{2+}, H_2pipz^{2+}, and $HDMA^+$ cations.

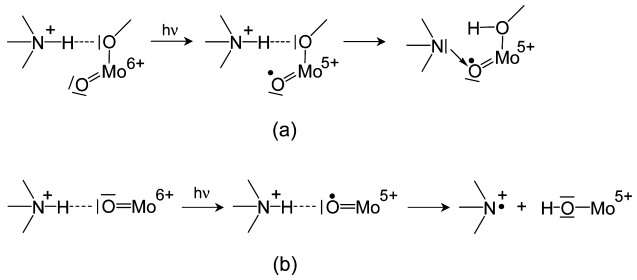

Figure 2. Mechanisms of photochromism in the organoammonium−POM hybrid materials involving (a) heterolytic dissociation and (b) homolytic dissociation of the N^+-H bond of the $N^+-H\cdots O$ hydrogen bond.

organoammonium−POM hybrid materials, which proposes proton transfer in the $N^+-H\cdots O$ hydrogen bonds from the organoammonium cation to the POM block after Mo^{6+} cations are photoreduced to Mo^{5+} cations under UV irradiation (see Figure 2a). Compounds containing only ammonium cations, e.g., $(NH_4)_6[Mo_7O_{24}]\cdot 4H_2O$,[3] $(NH_4)_4[Mo_8O_{26}]$,[4] and $(NH_4)_6[Mo_8O_{27}]\cdot 4H_2O$,[5] do not show any UV−visible photoinduced color change. Thus, for photochromism in **1** only the H_2DABCO^{2+} cations in site 1 are responsible. Photogeneration of the colored state is significantly faster for **2** and **3** than for **1** (see below). This may originate from two factors. First, the H_2pipz^{2+} cation has a greater ability to free one proton under excitation than does the NH_4^+ cation. Second, site 2 provides a faster response of the cations to a photostimulus than does site 1 for geometrical reasons. The latter is corroborated by the fact that the photochromic responses of **2** and **3** are very similar.[2] This would stem from the nature of the oxygen atom of the POM block involved in the $N^+-H\cdots O$ hydrogen bonds, i.e., a terminal oxygen atom at site 2 and a bridging oxygen atom at site 1. This reasoning implies further that the speed of the photoinduced color change can be tuned in the $(H_2DABCO)_2(A)_x[Mo_8O_{27}]\cdot nH_2O$ (A = organoammonium cations) hybrid series with a proper choice of the cations located at site 2.

In the present work we explore the above implications by investigating what features of an organoammonium−POM hybrid material govern the photochromic response. Photochromism in such materials occurs most frequently with secondary organoammonium cations,[6] and $(HDMA)_4[Mo_6O_{20}]\cdot 2H_2O$[7] is the most efficient material as far as the rapidity of the color change is concerned.[1] Thus, we embarked on the synthesis of the $(H_2DABCO)_2(HDMA)_2[Mo_8O_{27}]\cdot nH_2O$ compound. This effort led to the preparation of $(H_2DABCO)_2(HDMA)_{0.5}Na_{0.75}(H_3O)_{0.75}[Mo_8O_{27}]\cdot 3H_2O$ (**4**), a new photochromic member of the $(H_2DABCO)_2(A)_x[Mo_8O_{27}]\cdot nH_2O$ series with a strong photoresponse to UV−visible photostimulation. In what follows the kinetics of photoinduced coloration in **1**−**4** under UV−visible illumination is analyzed, and the mechanism of photochromism is discussed on the basis of first-principles density functional theory (DFT) calculations. Our work shows that the photochromism of **1**−**4** involves hydrogen transfer rather than proton transfer in the $N^+-H\cdots O$ hydrogen bonds and that the event of light absorption at a reducible Mo^{6+} site does not necessarily coincide with that of the N^+-H bond breaking in the $N^+-H\cdots O$ hydrogen bond associated with the Mo^{6+} site. The model of photochromism resulting from our work differs slightly from Yamase's model and accounts for the experimental trends observed in the whole series of organoamonium−POM hybrid materials investigated herein.

Experimental Section

Synthesis. 1,4-Diazabicyclo[2.2.2]octane, $N_2C_6H_{12}$ (DABCO), dimethylamine hydrochloride, NC_2H_8Cl (DMA·HCl), and $Na_2MoO_4\cdot 2H_2O$ were purchased from Aldrich. All reagents were used without further purification. $Na_2MoO_4\cdot 2H_2O$ (3.388 g, 14 mmol) was dissolved in 30 mL of water. After addition of DABCO (0.392 g, 3.5 mmol) and DMA·HCl (1.141 g, 14 mmol), the pH was adjusted with 1 M HCl until it reaches 4. The mixture was stirred at room temperature for 3 h and then filtered to isolate a pale yellow solid of **4**. The powder was washed with H_2O, EtOH, and Et_2O (yield 95%). Anal. Calcd for $C_{13}H_{40.25}O_{30.75}N_{4.5}Na_{0.75}Mo_8$: C, 10.16; H, 2.64; N, 4.10; Na, 1.12; Mo, 49.95. Found: C, 10.19; H, 2.60; N, 4.04; Na, 1.10; Mo, 49.53. FT-IR (cm^{-1}): H_2O, 1634 (w); H_2DABCO^{2+}, $HDMA^+$ cations, 1494 (w), 1473 (m), 1461 (m), 1395 (m), 1321 (m), 1285 (w), 1217 (sh), 1156 (w), 1057 (m), 1021 (sh), 977 (w); ν(Mo=O), ν(Mo−O−Mo), 931 (m), 875 (vs), 853 (s), 840 (s), 787 (m), 699 (vs), 650 (s), 575 (m), 546 (m), 525 (m), 501 (m), 477 (m), 440 (w).

Physical Measurements. FT-IR spectra were recorded in the 4000−400 cm^{-1} range on a BRUKER Vertex equipped with an attenuated total reflection (ATR) device from Specac Eurolabo and computer control using the OPUS software. Differential scanning calorimetry (DSC) and thermogravimetric analysis (TGA) were performed by flowing dry argon with a heating and cooling rate of 5 °C/min on a SETARAM Tg-DSC 111 between 20 and 800 °C. Room-temperature UV−visible diffuse reflectivity spectra were collected on a finely ground sample with a Cary 5G spectrometer (Varian) equipped with a 60 mm diameter integrating sphere and computer control using the "Scan" software. Diffuse reflectivity was measured from 250 to 1550 nm (i.e., from 5 to 0.8 eV) with a 2 nm step using Halon powder (from Varian) as a reference (100% reflectance). Samples of **1**−**4** were irradiated with a Fisher Bioblock labosi UV lamp (λ_{exc} = 365 nm, P = 12W).

(3) Lindqvist, I. *Acta Crystallogr.* **1950**, *3*, 159–160.
(4) Benchrifa, R.; Leblanc, M.; de Pape, R. *Eur. J. Solid State Inorg. Chem.* **1989**, *26*, 593–601.
(5) Böschen, V. I.; Buss, B.; Krebs, B. *Acta Crystallogr.* **1974**, *B30*, 48–56.
(6) Arnaud-Neu, F. Ph.D. Thesis, University of Strasbourg, France, 1973.
(7) Toraya, H.; Marumo, F.; Yamase, T. *Acta Crystallogr.* **1984**, *B40*, 145–150.

Table 1. Homolytic (E_{homo}) and Heterolytic (E_{hetero}) Dissociation Energies Calculated for the N^+-H Bonds of Some Organoammonium Cations and the O^+-H bond of H_3O^+

cation	E_{homo} (eV)	E_{hetero} (eV)
$HDMA^+$	4.667	10.194
H_2pipz^{2+}	4.850	5.605
H_2DABCO^{2+}	4.898	5.838
NH_4^+	5.872	9.266
H_3O^+	6.599	7.502

Theoretical Calculations. First-principles DFT calculations were carried out to estimate the homolytic (E_{homo}) and heterolytic (E_{hetero}) dissociation energies of the N^+-H bonds in cations $HDMA^+$ ($NC_2H_8^+$, dimethylammonium), H_2pipz^{2+} ($N_2C_4H_{12}^{2+}$, piperazinium), H_2DABCO^{2+} ($N_2C_6H_{14}^{2+}$, diprotonated 1,4-diazabicyclo-[2.2.2]octane), and NH_4^+ using the Gaussian 03 B.04 package.[8] In our calculations for E_{homo} and E_{hetero}, the geometries of the cations as well as their fragments were fully optimized by employing the B3LYP exchange functional[9] with the 6-31G* and 6-311G* basis sets, the B3P86 functional[10] with the 6-311++G(d,p) basis set, and the Perdew− Burke−Ernzerhof functional[11,12] with the 6-311++G(d,p) basis set. Since all calculations provide the same trends, Table 1 lists only those calculations with the B3P86 functional and the 6-311++G(d,p) basis set. A rigorous ab initio treatment of the photochromic mechanism in hybrid organic−inorganic materials should involve a complete account for the organic−inorganic interface as well as stabilization of the photogenerated colored state with its associated geometrical relaxation. However, such a treatment is impossible to achieve at present. Calculation of E_{homo} and E_{hetero} enables us, though qualitatively, to address the problem of the photochromic mechanism in the present series

$$N^+-H \rightarrow N^{+\bullet} + {}^{\bullet}H,\ E_{homo} \quad (1a)$$

$$N^+-H \rightarrow N: + H^+,\ E_{hetero} \quad (1b)$$

Characterization of $(H_2DABCO)_2(HDMA)_{0.5}Na_{0.75}(H_3O)_{0.75}[Mo_8O_{27}]\cdot 3H_2O$ (4). **4** is precipitated as a yellowish-white powder from sodium molybdate aqueous solution containing a mixture of H_2DABCO^{2+} and $HDMA^+$ cations. Attempts to obtain crystals suitable for X-ray diffraction investigation have not been successful. Nevertheless, the presence of the infinite $^1/_\infty[Mo_8O_{27}]^{6-}$ chains is unambiguously evidenced by IR spectroscopy coupled to optical and synthesis observations and elemental analysis.

The IR spectrum of **4** is compared with those of $(H_2DABCO)_2(H_2pipz)[Mo_8O_{27}]$ (**2**) and $(H_2pipz)_3[Mo_8O_{27}]$ (**3**) in Figure 3. The absorption bands of H_2DABCO^{2+} and $HDMA^+$ cations are located between 1500 and 1000 cm^{-1}. The existence of $^1/_\infty[Mo_8O_{27}]^{6-}$ entities in **4** is indicated by the $\nu(Mo{=}O_t)$ and $\nu(Mo-O-Mo)$ absorption bands at 931, 875, 853, 840, 787, 699, 650, 575, 546, 525, 501, 477, and 440 cm^{-1}, which match perfectly well with those of **2** (932, 875, 860, 839, 780, 701, 648, 576, 553, 534, 517, 474, and 438 cm^{-1}) and **3** (933, 873, 858, 845, 783, 707, 641, 578, 556, 534, 510, 482, and 443 cm^{-1}). Note that the structures of **2** and **3** were well characterized by single-crystal X-ray diffraction.[13,14] The

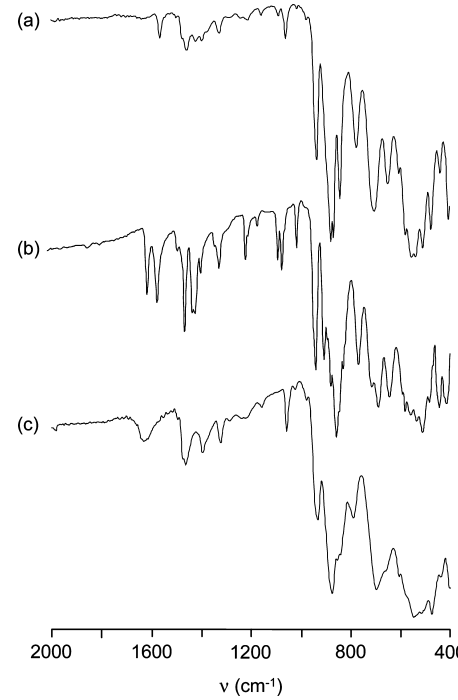

Figure 3. Comparison between the IR spectra of (a) $(H_2DABCO)_2(H_2pipz)[Mo_8O_{27}]$ (**2**), (b) $(H_2pipz)_3[Mo_8O_{27}]$ (**3**), and (c) $(H_2DABCO)_2(HDMA)_{0.5}Na_{0.75}(H_3O)_{0.75}[Mo_8O_{27}]\cdot 3H_2O$ (**4**).

presence of $^1/_\infty[Mo_8O_{26}]^{4-}$ and $^1/_\infty[Mo_3O_{10}]^{2-}$ chains as well as $[Mo_7O_{24}]^{6-}$ discrete entities in **4** can be discarded due to significant mismatches in the IR spectra of **4** with $(H_2DABCO)_2[Mo_8O_{26}]\cdot 4H_2O$, $(H_2DABCO)[Mo_3O_{10}]\cdot H_2O$, and $(H_2DABCO)_3[Mo_7O_{24}]\cdot 4H_2O$.[2]

The optical band gap of **4** in its ground state is identical with those of **1**, **2**, and **3** (3.1 eV) but differs significantly from those of $(H_2DABCO)_3[Mo_7O_{24}]\cdot 4H_2O$ (3.4 eV) and $(H_2DABCO)[Mo_3O_{10}]\cdot H_2O$ (3.5 eV).[2] Furthermore, **1**−**4** shift from white to purple under UV illumination (at 365 and 254 nm), while the photogenerated state of $(H_2DABCO)_3[Mo_7O_{24}]\cdot 4H_2O$ and $(H_2DABCO)[Mo_3O_{10}]\cdot H_2O$ is pale pink and reddish brown in color, respectively. $(H_2DABCO)_2[Mo_8O_{26}]\cdot 4H_2O$, containing the infinite $^1/_\infty[Mo_8O_{26}]^{4-}$ chains, has an optical band gap (around 3.0 eV)[2] similar to those of **1**−**4** but is not photochromic at all. Thus, **4** cannot have the infinite $^1/_\infty[Mo_8O_{26}]^{4-}$ chains.

The presence of infinite $^1/_\infty[Mo_8O_{27}]^{6-}$ chains in **4** is also consistent with the synthetic conditions employed. As discussed previously,[2] stabilization of polyoxomolybdate in hybrid solids is strongly dependent on the pH. While the infinite $^1/_\infty[Mo_8O_{26}]^{4-}$ chain and the discrete $[Mo_7O_{24}]^{6-}$ cluster are stable in a large range of pH (1−3 and 4.5−7, respectively), syntheses of $^1/_\infty[Mo_8O_{27}]^{6-}$ containing hybrid materials **1**, **2**, and **3** at room temperature occur only for pH around 4 in the presence of organoammonium cations with at least two N−H bonds. The synthetic condition of **4** is similar to those of **1** and **2** except for use of $HDMA^+$ instead of NH_4^+ and H_2pipz^{2+}.

4 contains H_2DABCO^{2+} and $HDMA^+$ cations as well as water molecules and H_3O^+ cations. Formally, chemical analysis of **4** leads to the composition $(C_6N_2H_{14})_2(C_2NH_8)_{0.5}Na_{0.75}(H_3O)_{0.75}[Mo_8O_{27}]\cdot 3H_2O$, hereafter labeled $(H_2DABCO)_2(HDMA)_{0.5}Na_{0.75}(H_3O)_{0.75}[Mo_8O_{27}]\cdot 3H_2O$, where the presence of H_3O^+ cations is assumed to balance the charge. DSC/TGA analyses displayed a continuous weight loss with temperature up to total deterioration of the material,

(8) Frisch, M. J.; et al. *Gaussian 03*, Revision B.04; Gaussian, Inc.: Pittsburgh, PA, 2003.
(9) Becke, A. D. *J. Chem. Phys.* **1993**, *98*, 5648–5652.
(10) Perdew, J. P. *Phys. Rev. B* **1986**, *33*, 8822–8824.
(11) Perdew, J. P.; Burke, K.; Ernzerhof, M. *Phys. Rev. Lett.* **1996**, *77*, 3865–3868.
(12) Perdew, J. P.; Burke, K.; Ernzerhof, M. *Phys. Rev. Lett.* **1997**, *78*, 1396.
(13) Wang, R.-Z.; Xiao, L.; Wang, Y.-Y.; Ma, C.-H.; Du, J.; Lin, X.; Liu, C.-L. *Solid State Sci.* **2006**, *8*, 77–81.
(14) Harrison, W. T. A.; Dussack, L. L.; Jacobson, A. J. *Acta Crystallogr.* **1996**, *C52*, 1075–1077.

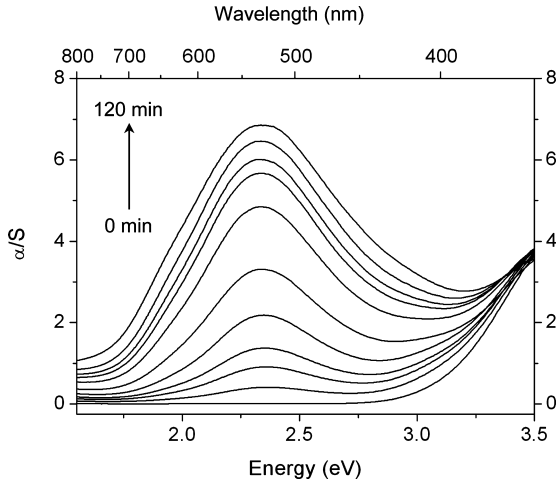

Figure 4. Kubelka−Munk transformed reflectivity of **4** after 0, 1, 2, 3, 5, 10, 20, 30, 40, 60, and 120 min of irradiation at 365 nm.

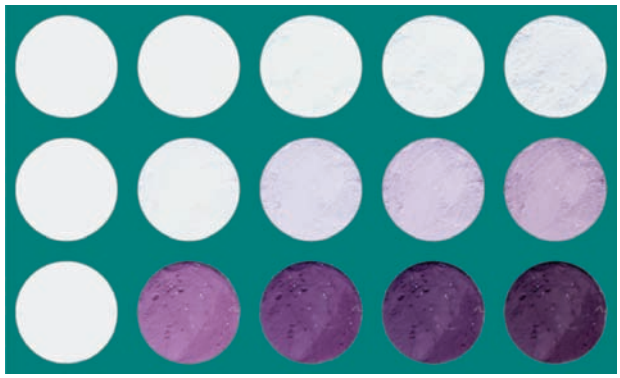

Figure 5. Color of **1** (first row), **2** (second row), and **4** (third row) after 0, 5, 20, 50, and 140 min irradiation (from left to right) at 365 nm. **2** and **3** display very similar optical behaviors.

which prevents us from determining the content of water molecules in **4**. The presence of Na^+ cations should result from the precursors. Attempts to prepare stoichiometric $(H_2DABCO)_2(HDMA)_2[Mo_8O_{27}]\cdot nH_2O$ have not been successful so far, even with introducing $HDMA^+$ cations in large excess and substituting the Na^+-free precursor MoO_3 for $Na_2MoO_4\cdot 2H_2O$.

Irradiation Time Dependence of Absorption. The reflectivity data were treated by a Kubelka−Munk transformation to obtain the corresponding absorption data and hence better locate the absorption bands and absorption threshold. Our results for **4** are shown in Figure 4, which exhibits an optical band gap of 3.1 eV in agreement with its yellowish-white color in the ground state. Under UV excitation at 365 nm (3.4 eV), **4** shows first a faint purple color and then rapidly darkens with increasing irradiation time. This color change is associated with the rise of a broad band peaking at 525 nm (2.36 eV). With the naked eye, the color change can be perceived after 10 s of daylight illumination. As expected, the optical characteristics of **4** are similar to those of **1**, **2**, and **3**.[2] Hence, the compounds **1**−**4** have an identical absorption threshold at 3.1 eV and an identical photogenerated absorption band centered at 2.36 eV, which originates from the presence of the $^1/_\infty[Mo_8O_{27}]^{6-}$ chains in the four materials. Nevertheless, materials **1**−**4** differ considerably in their kinetics of coloration as can be seen from Figure 5, which shows the color change in **1**, **2**, and **4** after UV irradiation at 365 nm for several different lengths of time.

Kinetics of Coloration. In this section we quantify the kinetics of the coloration in **1**−**4** by analyzing their reflectivity values $R(t)$ in the range of 350−800 nm as a function of the irradiation time t. The wavelength dependence of $R(t)$ determined for **4** at various irradiation time t is summarized in Figure 6. The corresponding plots made for **1**−**3** are given as Figures S1−S3 in the Supporting Information. The sweeping time of the reflectivity measurements for the range of 350−800 nm is 20 s, which is much shorter than the time interval between successive irradiation times. Practically, there is no change in the values of the reflectivity after the sweeping. For our analysis, we choose the $R(t)$ vs t relationship at 525 nm (2.36 eV) where the maximum absorption of the photoinduced state occurs (Figure 4). The $R(t)$ vs t relationships for **1**−**4** are summarized in Figure 7.

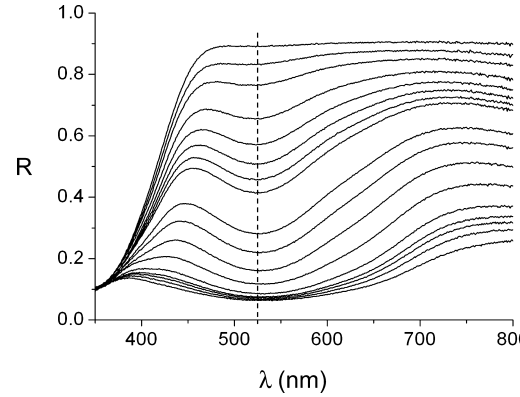

Figure 6. Reflectance $R(t)$ of **4** in the 350−800 nm range measured after irradiating the sample for t min with UV light at 365 nm. The vertical dashed line at 525 nm indicates that the local minimum of the reflectance occurs at 525 nm.

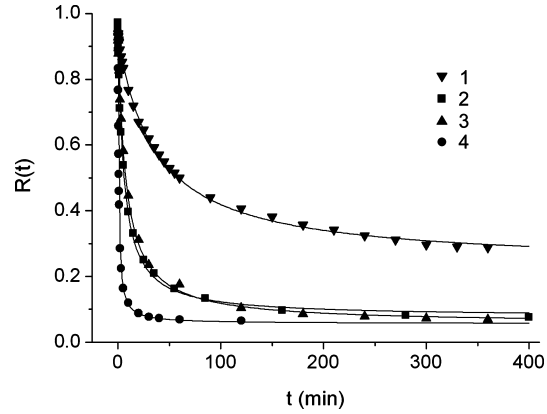

Figure 7. Reflectivity $R(t)$ vs t plots for **1**−**4** measured at 525 nm.

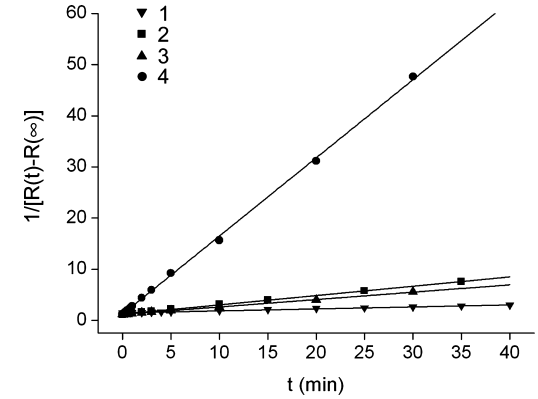

Figure 8. $1/[R(t) - R(\infty)]$ vs t plots for **1**–**4**.

The appearance of a photogenerated color in hybrid materials based on organoammonium cations and polyoxomolybdates is

related to a partial reduction of Mo^{6+} cations into Mo^{5+} cations. This reduction takes place only on the surface of the irradiated sample grains due to the low penetration depth of the incident light into the matter. Let us use $C_{6+}(0)$ for the concentration of Mo^{6+} at $t = 0$, i.e., at the time just before UV illumination. Given that photochromism requires displacement of hydrogen from the organic component toward the mineral framework under excitation,[1] it is reasonable to assume that only those Mo^{6+} ions in the $[MoO_6]$ octahedra connected to organoammonium cations via $N^+-H\cdots O$ hydrogen bonds are photoreduced. Before UV excitation, therefore, $C_{6+}(0)$ consists of two contributions, namely

$$C_{6+}(0) = C_{6+,r}(0) + C_{6+,ir}(0) \quad (2a)$$

where $C_{6+,r}(0)$ is the concentration of Mo^{6+} ions that are photoreducible and $C_{6+,ir}(0)$ that of Mo^{6+} ions that are photoirreducible either because their $[MoO_6]$ octahedra are not involved in forming $N^+-H\cdots O$ hydrogen bonds or because they are not present on the surface of sample grains. After illuminating for the duration of t, some reducible Mo^{6+} ions are converted to Mo^{5+} ions, so that

$$C_{6+}(0) = C_{6+,r}(t) + C_{5+}(t) \quad (2b)$$

where $C_{6+,r}(t)$ is the concentration of the remaining reducible Mo^{6+} ions at t and $C_{5+}(t)$ the concentration of Mo^{5+} ions at t. Therefore

$$C_{6+}(0) = C_{6+,ir}(0) + C_{6+,r}(t) + C_{5+}(t) \quad (2c)$$

It should be noted that at any irradiation time t, the absorption $A(t)$ and reflection $R(t)$ must satisfy

$$A(t) + R(t) = 1 \quad (3)$$

In our experiment the values of the reflectivity measurements for **1**−**4** were obtained using the reflectivity of halon as the reference. Thus, the $R(0)$ value is slightly smaller than 1 because halon is white while **1**−**4** are pale yellow so that halon has a stronger reflectivity and hence $A(0) = 1 - R(0)$ is nonzero. In general, at time t, two terms contribute to $A(t)$, namely, the "residual" absorption $A(0)$ plus the term that is proportional to the concentration of the photogenerated Mo^{5+} species,

$$A(t) = \alpha C_{5+}(t) + A(0) \quad (4)$$

where α is the proportionality constant. Thus, under UV excitation it is expected that $A(t)$ progressively increases and asymptotically approaches the limit $A(\infty)$, which is reached when all the photoreducible Mo^{6+} ions are converted to Mo^{5+} ions, i.e., $C_{5+}(\infty) = C_{6+,r}(0)$. From eqs 3 and 4, $R(t)$ is rewritten as

$$R(t) = R(0) - \alpha C_{5+}(t) \quad (5)$$

which combined with eq 2c becomes

$$R(t) = \alpha C_{6+,r}(t) + \{R(0) - \alpha[C_{6+}(0) - C_{6+,ir}(0)]\} \equiv \alpha C_{6+,r}(t) + R(\infty) \quad (6)$$

Thus, $R(t)$ will continuously decrease with increasing t to an asymptotic limit $R(\infty)$.

Let us now consider the event of light absorption at a reducible Mo^{6+} site and that of breaking the N^+-H bond of the $N^+-H\cdots O$ hydrogen bond connected to the Mo^{6+} site. If these two events are assumed to occur simultaneously then the change in $C_{6+,r}$ as a function of time is proportional to the concentration of the reducible Mo^{6+} sites, i.e., $iC_{6+,r}$, i.e.

$$\frac{dC_{6+,r}(t)}{dt} = -kC_{6+,r}(t) \quad (7a)$$

where k is the rate constant. Consequently,

$$C_{6+,r}(t) = C_{6+,r}(0)e^{-kt} \quad (7b)$$

According to this first-order reaction, $R(t)$ is expressed as an exponential function of t, i.e.

$$R(t) = \alpha C_{6+,r}(0)e^{-kt} + R(\infty) \equiv ae^{-kt} + b \quad (8)$$

where $a = \alpha C_{6+,r}(0)$ and $b = R(\infty)$. Our analysis shows that the $R(t)$ vs t relationships of **1**−**4** are not well fitted by eq 8 with two fitting parameters a and b.

This failure prompts us to abandon the assumption that every event of light absorption at a reducible Mo^{6+} site leads to N^+-H bond breaking of the $N^+-H\cdots O$ hydrogen bond associated with the Mo^{6+} site. Under irradiation, an electron is excited from the oxygen p-block levels to the d-block levels of a reducible Mo^{6+} site in POM and the excited electron may return to the oxygen p-block levels. Such excitation and de-excitation processes may occur repeatedly until the state of the N^+-H stretching vibration becomes favorable for the photoexcited state of the Mo^{6+} site to induce N^+-H bond breaking. In such a case, the rate of change in $C_{6+,r}$ as a function of time will be proportional not only to the concentration of the reducible Mo^{6+} sites but also to that of the N^+-H bonds associated with the Mo^{6+} sites. Since these two concentrations are equal, we have

$$\frac{dC_{6+,r}(t)}{dt} = -k[C_{6+,r}(t)]^2 \quad (9a)$$

where k is the rate constant. Consequently,

$$\frac{1}{C_{6+,r}(t)} = \frac{1}{C_{6+,r}(0)} + kt \quad (9b)$$

As a result,

Table 2. Values of the Fitting Parameters Describing the $R(t)$ vs t Relationships for 1−4

	1	2	3	4
$R(0)$	0.938	0.972	0.942	0.893
a	0.698 ± 0.005	0.884 ± 0.006	0.876 ± 0.005	0.853 ± 0.005
b	0.027 ± 0.001	0.180 ± 0.006	0.129 ± 0.004	1.311 ± 0.030
$R(\infty)$	0.232 ± 0.005	0.076 ± 0.005	0.055 ± 0.004	0.056 ± 0.003
R^{2a}	0.99889	0.99917	0.99947	0.99407
A	1.440 ± 0.008	1.176 ± 0.019	1.143 ± 0.017	1.164 ± 0.115
B	0.039 ± 0.001	0.183 ± 0.001	0.145 ±0.002	1.530 ± 0.011
R^{2a}	0.99700	0.99927	0.99882	0.99934
k_i/k_1	1.0 ± 0.0	4.7 ± 0.1	3.7 ± 0.1	39.2 ± 1.3
$t_{1/2}$ (min)	37.0 ± 1.4	5.6 ± 0.2	7.8 ± 0.2	0.8 ± 0.0

[a] Regression coefficient.

$$R(t) = \frac{\alpha C_{6+,r}(0)}{C_{6+,r}(0)kt + 1} + R(\infty) \equiv \frac{a}{bt + 1} + c \qquad (10)$$

where $a = \alpha C_{6+,r}(0)$, $b = kC_{6+,r}(0)$, and $c = R(\infty)$. This expression allows us to fit the $R(t)$ vs t relationships of **1**−**4** in terms of three fitting parameters a, b, and c. As shown by the solid lines in Figure 7, the $R(t)$ vs t relationships of **1**−**4** are very well fitted by eq 10. This reflects the reasonableness of the assumption that every event of light absorption at a reducible Mo^{6+} site does not necessarily break the N^+−H bond of the N^+−H···O hydrogen bond associated with the Mo^{6+} site. Namely, only when the two events occur simultaneously will the photogenerated electron be trapped at the molybdenum site.

The a, b, and $R(\infty)$ parameters obtained from the latter fitting analysis are tabulated in Table 2. For all compounds the $R(0)$ values are similar but the $R(\infty)$ values differ significantly. In particular, $R(\infty)$ is much larger for **1** than for **2**, **3**, and **4**, which is in agreement with the fact that the coloration of **1** under UV irradiation is less pronounced after a long irradiation exposure (i.e., lower capability to generate Mo^{5+} cations under illumination for **1** than for **2**, **3**, and **4**). To extract the rate constant k for **1**−**4** we rewrite eq 10 as

$$\frac{1}{R(t) - R(\infty)} = \frac{k}{\alpha}t + \frac{1}{\alpha C_{6+,r}(0)} \equiv Bt + A \qquad (11)$$

where $B = k/\alpha$ and $A = 1/\alpha C_{6+,r}(0)$. Thus, the plot of $1/[R(t) - R(\infty)]$ vs t should be linear with the slope k/α. This is indeed the case as shown in Figure 8, especially in the first 40 min of the irradiation time. In fact, the plot is linear in the first ∼210, ∼100, ∼120, and ∼40 min for **1**, **2**, **3**, and **4**, respectively. Beyond these time domains, the $1/[R(t) - R(\infty)]$ values deviate from the linear fitting because there is no more Mo^{6+} cation to be reduced since the photoreduction process is practically finished. The values of A and B for **1**−**4** extracted by fitting their $1/[R(t) - R(\infty)]$ vs t plots with eq 11 are also listed in Table 2. For convenience of our discussion, the symbols k_i, B_i, and A_i (i = 1−4) will be used to indicate the constants k, B, and A for compound i (= 1−4). For each compound i, the slope of the $1/[R(t) - R(\infty)]$ vs t plot gives the value $k_i/\alpha_i = B_i$, where the parameter α_i is unknown. However, it is reasonable to assume that the α_i (i = 1−4) are practically identical because **1**−**4** contain the same inorganic $^1/_\infty[Mo_8O_{27}]^{6-}$ chains and their photochromic properties are attributed to the occurrence of Mo^{5+} cations. Therefore, one can obtain the relative rate constants k_i/k_1 (i = 1−4) from the fitting parameters B_i, as listed in Table 1. Thus, the rates of the photocoloration in **2**, **3**, and **4** are enhanced from that of **1** by a factor of ∼5, ∼4, and ∼40, respectively. Namely, the speeds of the photoinduced color change increase in the order **1** < **3**, **2** < **4**. An alternative way of comparing the speeds of photoinduced coloration for **1**−**4** is to consider the half-life $t_{1/2}$, namely, the time required for $R(t)$ to reach the $[R(0) + R(\infty)]/2$ value. According to eq 10, $t_{1/2}$ is given by

$$t_{1/2} = \frac{1}{b} \qquad (12)$$

which is readily obtained from the b value already found. The values of $t_{1/2}$ for **1**−**4** are summarized in Table 2, which shows that the speeds of photoinduced color change increase in the order **1** < **3**, **2** < **4**, as found from the relative rate constants k_i/k_1.

Theoretical Considerations of Photochromism. As depicted in Figure 2a, Yamase's model of photochromism supposes that UV−vis excitation transfers an electron from a terminal oxygen atom of the POM block to the adjacent Mo^{6+} ($4d^0$) site. Subsequently, this is followed by proton transfer along the N^+−H···O hydrogen bond from the N^+ to the O atom and simultaneously the resulting amine N atom interacts with the hole left on the terminal O to form a charge-transfer complex. It is the occurrence of Mo^{5+} ($4d^1$) cations that explains the generation of a colored state because it induces d−d excitations as well as $Mo^{5+} \rightarrow Mo^{6+}$ intervalence charge-transfer transitions. According to this model, the kinetics of photoinduced coloration in **1**−**4** should be correlated to E_{hetero} defined as the energies required to induce the heterolytic breaking of the N^+−H bonds of the organoammonium cations (eq 1b), so that the hybrid material with faster speed of photoinduced color change should have the organoammonium cation with a lower E_{hetero}. To test the above prediction we calculated the E_{hetero} values for the cations $HDMA^+$, H_2pipz^{2+}, H_2DABCO^{2+}, NH_4^+, and H_3O^+ on the basis of first-principles DFT calculations. As can be seen from Table 1, these energies cannot explain the experimental observation that the speeds of the photoinduced color change increase in the order **1** < **3**, **2** < **4**.

An alternative process of photochromism, displayed in Figure 2b, supposes the homolytic cleavage of the N^+−H bond (eq 1a) to stabilize the photogenerated hole on the oxygen atom of the POM block. (The terminal oxygen on the POM might be replaced by a bridging oxygen without changing the significance of the model.) The E_{homo} values increase in the order $HDMA^+ < H_2pipz^{2+} < H_2DABCO^{2+} < NH_4^+ < H_3O^+$. As the E_{homo} value of the cation decreases, the speed of the photoinduced coloration containing that cation is expected to increase. Indeed, this expectation is borne out; the relative rate constants k_i/k_1 of **1**−**4** decrease with increasing the E_{homo} values of their organoammonium cations (Figure 9a), and the half-lives $t_{1/2}$ increase with increasing the E_{homo} values (Figure 9b). At this stage it should be emphasized that only H_2DABCO^{2+}

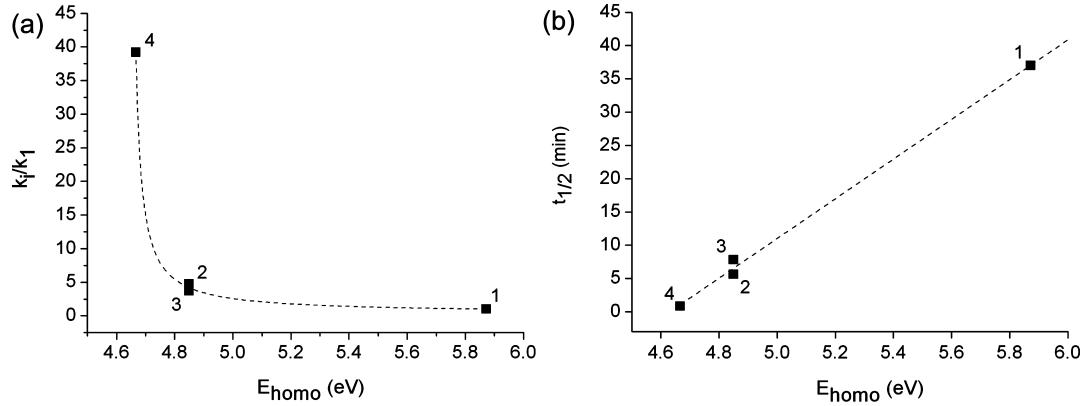

Figure 9. (a) k_i/k_1 and (b) $t_{1/2}$ of **1**−**4** vs E_{homo} of their organoammonium cations in lattice site 2.

cations in lattice site 1 are at work in the photoinduced coloration of **1**. In the coloration of **2** and **4**, the rate is strongly enhanced because H_2DABCO^{2+} and $HDMA^+$ in lattice site 2 have a smaller E_{homo} value than does NH_4^+. **2** and **3** are similar in the coloration rates because H_2DABCO^{2+} and H_2pipz^{2+} have similar E_{homo} values and lattice site 1 is much less photoactive than lattice site 2.

The E_{homo} values of Table 1 show that homolytic bond dissociation is very difficult for NH_4^+ and H_3O^+, and hence, these cations may not give rise to photochromism in materials in which they are associated with the POM blocks.[1] In addition, Table 1 shows that for a given organoammonium cation, the homolytic dissociation of the N^+-H bond requires less energy than does the heterolytic dissociation of the N^+-H bond. The mechanism proposed in Figure 2b predicts the generation of both organic cation and inorganic anion radicals, while Yamase's model suggests the occurrence of a delocalized electron on the N···O bond (Figure 2a) or a radical on the amine molecule concomitantly with an unpaired electron on Mo^{5+} cations. The presence of the inorganic radicals is readily detected by EPR, but that of the organic radical is not. The latter probably means that the relaxation time of the organic radical is very short in organoammonium−POM salts.

Concluding Remarks

The present work shows that the speed of photoinduced color change in the organoammonium−POM hybrids $(H_2DABCO)_2(A)_x[Mo_8O_{27}]\cdot nH_2O$ (A = countercations) can be tuned substantially by changing the nature of the organoammonium cation A at site 2 and that the mechanism of the photochromism in these compounds involves homolytic dissociation of the N^+-H bonds associated with the $N^+-H\cdots O$ hydrogen bonds (Figure 2b). The rates of the photoinduced color change in **1**−**4** are well described by the second-order kinetic equation, which indicates that the event of light absorption at a reducible Mo^{6+} site does not necessarily coincide with that of the N^+-H bond breaking associated with the Mo^{6+} site. It is hoped that our study stimulates the synthesis of organic−inorganic hybrid materials with fast photochromic response. At this stage the effect of the organic−inorganic interface on the photochromism of organoammonium−POM hybrid materials is not fully understood because of its structural complexity. Nevertheless, our work indicates that the photochromism requires the ability of the organic cation to donate one hydrogen atom to the inorganic block. Thus, the homolytic dissociation energy of the N^+-H bond should be small and the geometrical feature of the $N^+-H\cdots O$ hydrogen bond should be favorable for hydrogen transfer.

Acknowledgment. M.-H.W. is thankful for support of the Office of Basic Energy Sciences, Division of Materials Sciences, U.S. Department of Energy, under Grant DE-FG02-86ER45259.

Supporting Information Available: Evolution of the reflectance $R(t)$ of **1**, **2**, and **3** in the 350−800 nm range measured after irradiating the sample for t min with UV light at 365 nm. The dashed line indicates the local minimum reflectance. This material is available free of charge via the Internet at http://pubs.acs.org.

IC8013865